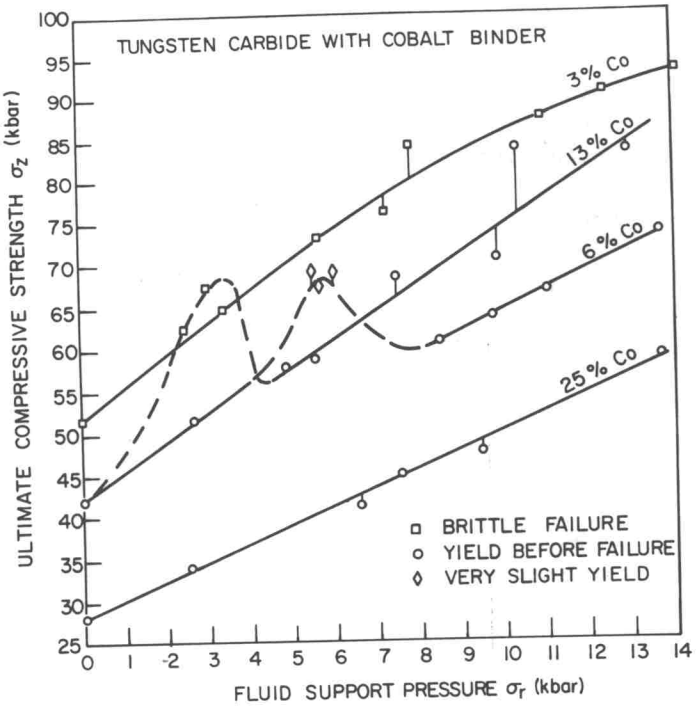

Fig. 3 Variation of ultimate compressive strength as a function of fluid support pressure for tunsten-carbide materials with cobalt binder

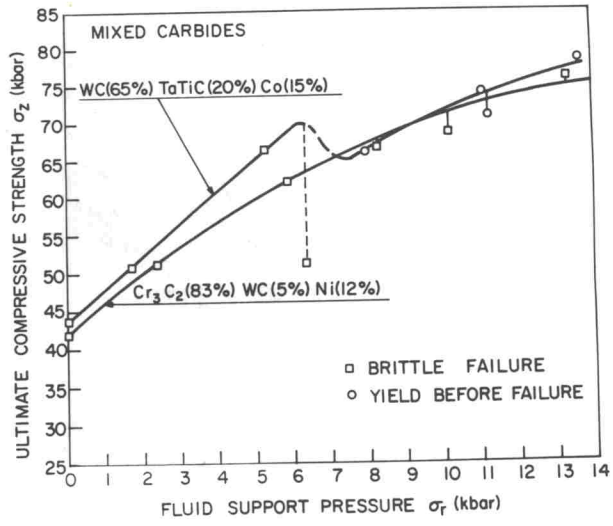

Fig. 4 Variation of ultimate compressive strength as a function of fluid support pressure for two mixed carbide materials

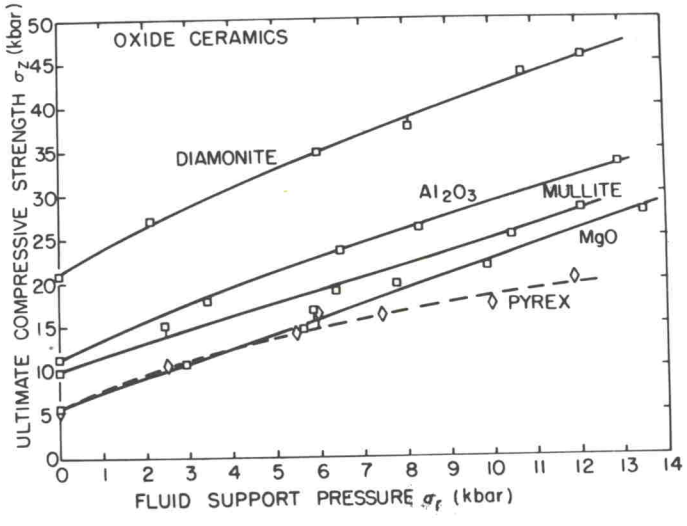

Fig. 5 Variation of ultimate compressive strength as a function of fluid support pressure for various oxide ceramics

counted for by considering the linear compression of the component parts (spacers, piston, seals, and driving ram) of the travel monitoring system. The relative changes in length of the specimens were small (<2 percent) and the associated changes in cross-sectional area were ignored in the calculations. In experiments typified by curve B of Fig.2, the increase in slope at the yield point must be attributed to specimen deformation. For most applications, deformations as large as those displayed by curve B between the yield point and the failure point would be undesirable; therefore, for specimens typified by curve B, the ultimate compressive strength reported was calculated at the yield point ignoring specimen deformation occurring before the yield point. The data for both types of specimens were reduced in the same way, substituting the yield point for the failure point when the specimen exhibited yielding.

The hydrostatic support pressure at the failure point was obtained in the following manner. The hydrostatic support pressure at the contact point may be obtained from the apparatus calibration and the ram pressure at the contact point (P_c). The hydrostatic support pressure at the failure point was somewhat higher than at the contact point. Two factors enter into an estimate of this increase in support pressure. The first is an estimate of the advance of the pressure seal based on the compressibilities of the spacers and sealing piston. The second is an estimate of the increase in fluid pressure owing to the advance of the seal. Consideration of the ratio of the cross-sectional area of the spacers to the cross-sectional area of the pressure chamber indicates the rate of increase in fluid pressure per unit increase in piston advance to be decreased by a factor of seven compared to the rate before the contact point was reached. In this way a small incremental increase in applied ram pressure (ΔP) corresponding to the increased flu-

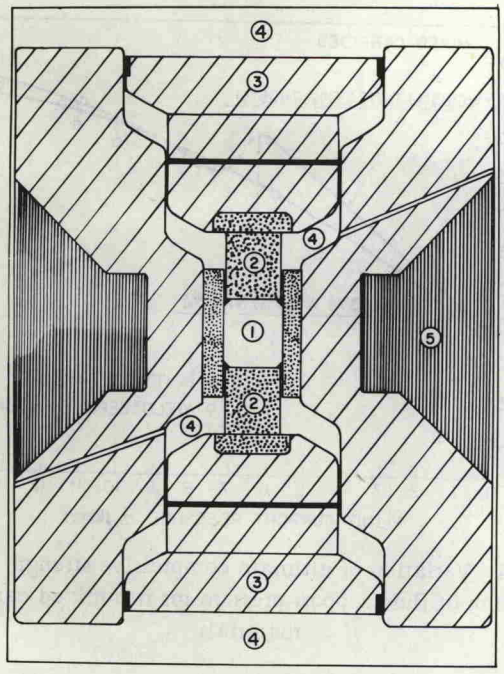

Fig. 6 Schematic representation of large volume high-pressure apparatus employing fluid enhancement of ultimate compressive strength of piston. Components are shown within chamber of a large autoclave: (1) sample, (2) fluid supported WC pistons, (3) driving piston, (4) hydrostatic fluid, and (5) lateral support mechanism

id pressure was estimated, and the hydrostatic support pressure at the failure point (σ_r) was taken to be the value corresponding to $P_c + \Delta P$ on the apparatus calibration curve.

The axial compressive stress on the specimen at failure was obtained by considering the ratio of the driving ram cross-sectional area to the specimen cross-sectional area (256:1). The ultimate compressive strength or axial compressive stress of the specimen at failure (σ_z) may thus be expressed as

$$\sigma_z = 256\ (P_u - P_c - \Delta P) + \sigma_r$$

where P_u is the applied ram pressure at the failure point or at the yield point for specimens which yielded before failure.

In this manner the experimental data, typified by the curves in Fig.2, were reduced to obtain the ultimate compressive strength (σ_z) as a function of hydrostatic support pressure (σ_r).

RESULTS AND DISCUSSION

The materials tested in these experiments were of three types: (1) Tungsten carbide with cobalt binder, (2) mixed carbides, and (3) oxide ceramics. The reduced data (σ_z versus σ_r) for the individual materials of each type are displayed in Figs.3, 4, and 5. The scatter of some of the data points was much too large to be attributed to the uncertainties of the measurement procedures and must be attributed to variations in the properties of the materials from specimen to specimen.

Tungsten Carbide with Cobalt Binder, Fig.3

These materials were purchased from the American Carbide Company in the final specimen configuration. The 3 percent cobalt binder, 6 percent cobalt binder, 13 percent cobalt binder, and 25 percent cobalt binder specimens were Amcarb grades D-5, D-20, D-40, and D-25, respectively. The specimens of tungsten carbide with 3 percent cobalt binder exhibited brittle failure at all support pressures tested, and the highest ultimate compressive strength observed was ~93 kbar with 14.1 kbar support pressure. The specimens of tungsten carbide with 6 percent cobalt binder exhibited varying degrees of yielding at all pressures. The amount of yielding was minimum near 6 kbar support pressure. The minimum in yielding is reflected by the hump in the σ_z versus σ_r curve near 6 kbar support pressure. The specimens of tungsten carbide with 13 percent cobalt binder also exhibited varying degrees of yielding. With zero support pressure slight yielding was observed. With approximately 3 kbar support pressure the specimens exhibited brittle fracture. With support pressures greater than 4 kbar, considerable yielding of the specimens and scatter in the data were observed. This variation in yielding produced a hump in the σ_z versus σ_r curve similar to that observed for the 6 percent cobalt binder specimens. The specimens of tungsten carbide with 25 percent cobalt binder yielded at all pressures. The amount of yielding increased with increasing support pressure.

Mixed Carbides, Fig.4

These materials were purchased from Metal Carbides Corporation in the final specimen configuration. The 65 percent tungsten carbide, 20 percent tantalum titanium carbide, 15 percent cobalt binder specimens were Talide grade CT-85. The 83 percent chrome carbide, 5 percent tungsten carbide, 12 percent nickel binder specimens were Talide grade CR-83. The tungsten-tantalum-titanium carbide specimens exhibited brittle failure at support pressures less than 6 kbar and yielded before failing at higher pressures. The low data point at 6.3 kbar support pressure was presumed